PHYSICAL REVIEW B 93, 161413(R) (2016)

Single-dot absorption spectroscopy and theory of silicon nanocrystals

Ilya Sychugov,[1,*] Federico Pevere,[1] Jun-Wei Luo,[2] Alex Zunger,[3] and Jan Linnros[1]

[1]Materials and Nano Physics Department, KTH–Royal Institute of Technology, Kista, Stockholm 16440, Sweden

[2]State Key Laboratory for Superlattices and Microstructures, Institute of Semiconductors, Chinese Academy of Sciences, P.O. Box 912, Beijing 100083, China

[3]Renewable and Sustainable Energy Institute, University of Colorado, Boulder, Colorado 80309, USA

(Received 30 November 2015; revised manuscript received 16 February 2016; published 26 April 2016)

Photoluminescence excitation measurements have been performed on single, unstrained oxide-embedded Si nanocrystals. Having overcome the challenge of detecting weak emission, we observe four broad peaks in the absorption curve above the optically emitting state. Atomistic calculations of the Si nanocrystal energy levels agree well with the experimental results and allow identiÞcation of some of the observed transitions. An analysis of their physical nature reveals that they largely retain the indirect band-gap structure of the bulk material with some intermixing of direct band-gap character at higher energies.

represent a mix of bulk bands over different wave vectors and band indices [1,2]. The additional shift in energies present in nanostructures due to quantum conÞnement and enhanced many-electron interactions in conÞned space lead to clear spectroscopic manifestations in nanostructures relative to the reference bulk material [3]. This includes changing of a bulk indirect transition to a nanostructure quasidirect transition [4], as well as more exotic effects such as Coulomb and spin blockade, appearance of many-electron multiplets, violations of HundÕs rule and the Aufbau principle, etc. [5]. The modern theory of nanostructures treats such single nanostructures atomistically as a giant molecule rather than via continuum-based effective mass methods [3,6]. However, such high-resolution theoretical calculations cannot be compared with experimental data from ensemble measurements, where size (and shape) dispersion even at a very small scale smears out discrete features both in emission and absorption. Single-dot spectroscopic techniques have been previously applied to self-assembled and colloidal

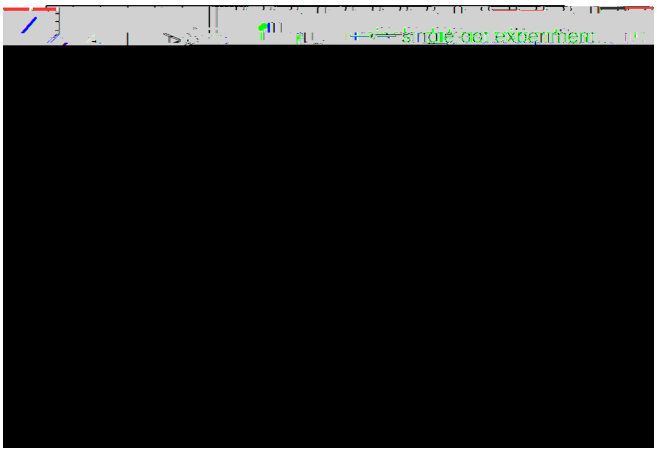

FIG. 1. Comparison of the experimentally obtained absorption curve (red circles to the right) with a calculated one (broadening 50 meV) for a 3 nm diameter Si nanocrystal (green curve) exhibiting best agreement. The room-temperature photoluminescence spectr (PL) of this nanodot is presented as red circles to the left. The PL peak position is close to the calculated band gap (green peak 1.88 eV). A typical featureless ensemble absorption [24] is also given for comparison (dashed line).

from Þtting to the experimental parameters of the bulk materia [29]. The no-phonon optical absorption spectrum in a single- particle basis was then calculated using FermiÕs golden ru where many-body effects are solved using a conÞguratio interaction (CI) approach [30]. Such an approach will help us to understand the origin of the spectral features observe experimentally in Si quantum dots. This theoretical method is summarized in the Supplemental Material and has been teste extensively over the past two decades for a broad range o spectroscopic quantities in colloidal as well as self-assemble nanostructures from the atomistic point of view [25,26,30].

In this work, theory and experiment are compared in a wide spectral range, from the emission peak position to th highest-energy absorption, pertaining to direct transitions This is illustrated in Fig. 1 by comparing the measured (red) and the calculated (green) absorption curves for a 3 nm Si nanocrystal. This nanodot has a calculated band gap o

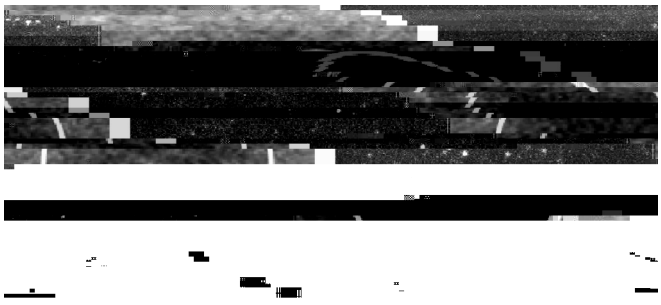

FIG. 2. Left: Cross-sectional TEM image of a silicon nanocrystal taken along the [110] direction from an SOI sample. Si (111) plane lattice fringes visible (scale bar 2 nm). Right: Photoluminescence image of $50 \times 50\,\mu m^2$ sample area. Bright points correspond to luminescence from individual Si quantum dots, formed randomly in a thinned SOI layer.

1.88 eV (green peak), similar to the measured PL peak position of 1.86 eV (red peak). Indeed, one can notice a good agreement over nearly three orders of magnitude in absorption intensity, where a growing curve with several discernible steps is predicted and observed experimentally. In this way, single-dot spectroscopy and atomistic calculations allowed us here to identify and analyze light absorbing states in indirect band-gap material nanocrystals.

The samples were fabricated by etching and short oxidation of silicon-on-insulator (SOI) wafers resulting in close to spherical, as well as faceted, silicon nanocrystals in an amorphous oxide matrix [4,31]. A typical transmission electron microscopy (TEM) image of such nanocrystals is shown in Fig. 2 (left). Interplane distance analysis reveals no signiÞcant

FIG. 3. Typical (top) room-temperature and (bottom) low-temperature photoluminescence (linewidth indicated) and absorption spectra of two different individual silicon quantum dots. Four steps on the absorption curves can be distinguished and the black line is a Þt based on four Gaussians (see text).

FIG. 5. Projections of the calculated conduction band states to bulk directlike Bloch functions for a 2.6 × 2.6 × 3 nm Si nanodot in oxide matrix. The intermixing of and X components is stronger for higher energy.

of the envelope functions with orbital angular momentum 0, 1, and 2 for holes and electrons in a silicon quantum dot). The next broad peak at 2.65 eV partially consists of the family of transitions. Higher-energy states of such nanodots were not analyzed in detail as they appear to consist of several mixed transitions from numerous, densely spaced electron and hole states. These states are highly quasidegenerate [25] and transitions between different sublevels result in broad experimental peaks (shown as a dashed line in Fig. 4, right), limited by the probe energy resolution and thermal broadening.

When analyzing these results we first notice that the absorption is very weak in the vicinity of the emission line (cf. Fig. 3). Indeed, the signal count rate for red light excitation was about two orders of magnitude lower than for blue light excitation, requiring a much longer time to get a measurable signal. To understand the nature of the absorbing states we calculated the conduction state wave-function projections to bulk Bloch functions (see the Supplemental Material). Since the initial valence band states are mostly localized around the point, the component of these projections represents the direct band-gap character of the transitions (Fig. 5). Indeed, the levels close to the emission energy retain the indirect nature of the bulk band gap (only admixture of the component), while at higher energies a strong intermixing of and states occurs (up to 30%). This situation is different from direct band-gap quantum dots, where strong direct band-gap related absorption peaks are located right next to the emission line [12–14].

This fact has a positive effect for the application of Si nanocrystals as phosphors in white-light emitting devices [16]. Indeed, from Fig. 3 one can see that within at least 300 meV next to the emission peak (110 nm for 1.8 eV) Si nanocrystals are nearly absorption free. The optimum positions of the trichromatic source for the generation of white light with a high color rendering index are at 450, 540, and 610 nm [33]. While the blue light in most modern white light-emitting diodes (LEDs) comes from an (In)GaN diode, the red and green bands originate from light converting phosphors. The 70 nm difference between the red and green bands is well within the poor absorption interval of Si nanocrystals. Thus the reabsorption for the green-red phosphor combination, which is a common problem for direct-band-gap nanocrystals [34], can be significantly reduced. Second, quantum dots have been recognized as superior biomarkers for multiplexing applications in biolabeling [35]. Here we note that the absorption at high energies is quite strong for Si nanocrystals due to the direct band-gap character admixture (Fig. 5), regardless of the emission energy, as shown recently for ensembles of ligand-passivated Si nanocrystals [36]. Such a large Stokes shift makes these nanoparticles good candidates for this application, considering the high natural abundance and the low toxicity of silicon.

In conclusion, we have measured absorption spectra of individual silicon nanocrystals in the visible range and found an energy structure consisting of several broad peaks, successfully reproduced by atomistic calculations. The origin of some peaks was identified as a convolution of transitions from different electron and hole states, including corresponding sublevels. The physics revealed by this single nanodot study of silicon is that the absorption states next to the emission level are still of an indirect band-gap nature, while at higher energies some intermixing with direct band-gap states occurs. For the application part, this large Stokes shift makes silicon nanocrystals attractive as phosphors and biolabels, where material abundance and nontoxicity are clear advantages.

Financial support from the Swedish Research Council (VR) through an individual contract (VR 2015-04064) and through a Linné grant (ADOPT) and from the Göran Gustafssons Foundation is gratefully acknowledged. J.W.L. was supported by the National Young 1000 Talents Plan and the National Science Foundation of China (NSFC Grant No. 61474116). The work of A.Z. was supported by Department of Energy, Office of Science, Basic Energy Science, MSE division under Grant No. DE-FG02-13ER46959 to CU Boulder.

[1] L. W. Wang, L. Bellaiche, S. H. Wei, and A. Zunger, Phys. Rev. Lett. 80

[12] D. Hessman, P. Castrillo, M. E. Pistol, C. Pryor, and L. Samuelson, Appl. Phys. Lett. 69, 749 (1996).
[13] Y. Toda, O. Moriwaki, M. Nishioka, and Y. Arakawa, Phys. Rev. Lett. 82, 4114 (1999).
[14] H. Htoon, P. J. Cox, and V. I. Klimov, Phys. Rev. Lett. 93, 187402 (2004).
[15] F. Sangghaleh, B. Bruhn, T. Schmidt, and J. Linnros, Nanotechnology 24, 225204 (2013).
[16] C.-C. Tu, J. H. Hoo, K. F. Boehringer, L. Y. Lin, and G. Cao, Opt. Express 22, A276 (2014).
[17] H. Nishimura et al., J. Cell Biol. 202, 967 (2013).
[18] S. Saeed, E. M. L. D. de Jong, K. Dohnalova, and T. Gregorkiewicz, Nat. Commun. 5, 4665 (2014).
[19] F. Sgrignuoli, P. Ingenhoven, G. Pucker, V. D. Mihailetchi, E. Froner, Y. Jestin, E. Moser, G. Sanchez, and L. Pavesi, Sol. Energy Mater. Sol. Cells 132, 267 (2015).
[20] M. T. Trinh, R. Limpens, W. D. A. M. de Boer, J. M. Schins, L. D. A. Siebbeles, and T. Gregorkiewicz, Nat. Photonics 6, 316 (2012).
[21] See Supplemental Material at http://link.aps.org/supplemental/10.1103/PhysRevB.93.161413 for experimental and calculation details.
[22] I. Sychugov, A. Fucikova, F. Pevere, Z. Yang, J. G. C. Veinot, and J. Linnros, ACS Photonics 1, 998 (2014).
[23] F. Pevere, I. Sychugov, F. Sangghaleh, A. Fucikova, and J. Linnros, J. Phys. Chem. C 119, 7499 (2015).
[24] F. Sangghaleh, I. Sychugov, Z. Yang, J. G. C. Veinot, and J. Linnros, ACS Nano 9, 7097 (2015).
[25] J.-W. Luo, P. Stradins, and A. Zunger, Energy Environ. Sci. 4, 2546 (2011).
[26] L. W. Wang and A. Zunger, Phys. Rev. B 54, 11417 (1996).
[27] H. X. Fu, L. W. Wang, and A. Zunger, Phys. Rev. B 57, 9971 (1998).
[28] J. W. Luo, S. S. Li, J. B. Xia, and L. W. Wang, Appl. Phys. Lett. 88, 143108 (2006).
[29] L. W. Wang and A. Zunger, Phys. Rev. B 51, 17398 (1995).
[30] V. Mlinar and A. Zunger, Phys. Rev. B 80, 205311 (2009).
[31] I. Sychugov, Y. Nakayama, and K. Mitsuishi, Nanotechnology 21, 5, 285307 (2010).
[32] J. Valenta, M. Greben, Z. Remes, S. Gutsch, D. Hiller, and M. Zacharias, Appl. Phys. Lett. 108, 023102 (2016).
[33] W. A. Thornton, J. Opt. Soc. Am. 61, 1155 (1971).
[34] X. Wang, X. Yan, W. Li, and K. Sun, Adv. Mater. 24, 2742 (2012).
[35] E. Petryayeva, W. R. Algar, and I. L. Medintz, Appl. Spectrosc. 67, 215 (2013).
[36] B. Lee, J. W. Luo, N. Neale, M. Beard, D. Hiller, M. Zacharias, P. Stradins, and A. Zunger, Nano Lett. 16, 1583 (2016).

Supplemental Material

Single-dot Absorption Spectroscopy and Theory of Silicon Nanocrystals

Ilya Sychugov, Federico Pevere, Jun-Wei Luo, Alex Zunger, Jan Linnros

A. Experiment: Silicon nanocrystals in an oxide matrix were produced by plasma etching and oxidation of low-doped silicon-on-insulator (SOI) wafers at 900^{o}C for 30 seconds. It was

increase the signal-to-noise ratio, results of two separate spectral scans were averaged. To acquire photoluminescence spectrum of a nanocrystal, the emitted light was dispersed in a spectrometer (Andor Shamrock) and recorded with the same CCD camera.

To extract the energy dependence of the absorption cross-section σ (cm^2) from the measured PL intensities, first we note that for a quantum dot below saturation the measured signal rate I_{det} (counts/sec) is directly proportional to the excitation photon flux Φ_{exc} (photons/cm^2/sec):

$$I_{det} = \sigma \cdot QY \cdot D \cdot \Phi_{exc} \quad (1),$$

where QY is the nanocrystal quantum yield and D is the system detectivity (counts/photon). We have experimentally verified the linearity of the signal rate dependence on the excitation power for the studied nanocrystals both at room and at low temperatures. Second, according to the Kasha-Vavilov rule, the quantum yield is excitation energy independent in this energy range, as it was recently verified experimentally for ligand-passivated Si nanocrystals [21]. Finally, the system detectivity is also a constant in this respect, since we detect the same emission line for all the excitation energies E. Thus the only varying parameters, which contribute to the energy dependence of the absorption cross-section σ (E), are the detected PL intensity I_{det} (E) and the excitation photon flux Φ_{exc} (E):

$$\sigma(E) \sim \frac{I_{det}(E)}{\Phi_{exc}(E)} \quad (2).$$

To obtain luminescence decay and rise times, necessary to find absolute values of the absorption cross-section, a modulated 405 nm laser diode (Omicron) was used for the excitation. In this experiment the photoluminescence signal was collected by an avalanche photodiode (ID Quantique) connected to another output port of the same microscope [S1]. In general, it can be shown from population rate equations that the luminescence rise rate Γ_{rise} is directly proportional to the excitation photon flux Φ_{exc} [

where the crystal potential of the NC plus its matrix are both described as a superposition of atomic screened (semi-empirical pseudopotential) potentials υ_α of atom type at each atomic site $R_{\alpha,n}$ within the lattice site n: $V(\mathbf{r}) = \sum_{\alpha,n} \upsilon_\alpha(\mathbf{r} - \mathbf{R}_{\alpha,n})$. The pseudopotentials υ_α are fitted to experimental transition energies, effective masses, and deformation potentials of the bulk material [28]. This atomistic empirical pseudopotential method takes into account inter-band coupling, inter-valley coupling (coupling between different parts of the Brillouin zone), and spin-orbit coupling. Although bulk Si has a very small spin-orbit interaction reflecting as small spin-orbit energy of 44 meV and its effect on the calculated spectra is expected to be negligible, in our atomistic calculations we still include the treatment of spin-orbit interaction. Because the continuum k·p effective mass approaches are extensively used in nanoscience and, in fact, the atomistic features of nanostructures usually play important roles in inter-band and inter-valley coupling, here we use "atomistic theory" term to emphasize the difference between our method with continuum k·p effective mass approach.

The no-phonon optical absorption spectrum $\alpha(\hbar\omega)$ in single-particle basis is calculated, given the dipole transition matrix $\overline{P}$, according to the Fermi-golden rule:

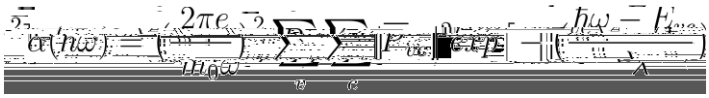

(5).

Here $E_{vc} = \epsilon_c - \epsilon_v$ is the transition energy from hole state v to electron state c, m_0 is the free-electron mass, and e is the free-electron charge, and λ represents the spectral line broadening.

$$H_{c,\,'c'} = \langle \Phi_{,c} | H_{CI} | \Phi_{',c'} \rangle = (\ _{c} - \ _{v})\ \ _{,\ '\ \ c,c'} - J_{\ c,\ 'c'222}$$

For the modelling of matrix a fictitious, lattice-matched barrier material having a wide band gap and large type-I band offsets with respect to bulk Si was introduced. Hence, the Si QDs calculated in this paper are a strain- and defect-free system relevant to the probed here optically active strain-free nanocrystals (Figure S1). The matrix material reproducing the experimentally measured bandgap of Si QDs in SiO_2

[S2] F. Priolo, G. Franzo, D. Pacifici, V. Vinciguerra, F. Iacona and A. Irrera “Role of the Energy Transfer in the Optical Properties of Undoped and Er-doped Interacting Si Nanocrystals” *J. Appl. Phys.* **89**, 264-272 (2001).

[S3] A. Franceschetti, H. Fu, L. W. Wang, and A. Zunger “Many-body Pseudopotential Theory of Excitons in InP and CdSe quantum dots” *Phys. Rev. B* **60**, 1819 (1999).